Bilayer Two-Orbital Model of $La_3Ni_2O_7$ under Pressure

Zhihui Luo, Xunwu Hu, Meng Wang, Wéi Wú, and Dao-Xin Yao*
Center for Neutron Science and Technology, Guangdong Provincial Key Laboratory of Magnetoelectric Physics and Devices, State Key Laboratory of Optoelectronic Materials and Technologies, School of Physics, Sun Yat-Sen University, Guangzhou, 510275, China

(Received 2 June 2023; revised 16 July 2023; accepted 23 August 2023; published 20 September 2023)

The newly discovered Ruddlesden-Popper bilayer $La_3Ni_2O_7$ reaches a remarkable superconducting transition temperature $T_c \approx 80$ K under a pressure of above 14 GPa. Here we propose a minimal bilayer two-orbital model of the high-pressure phase of $La_3Ni_2O_7$. Our model is constructed with the Ni-$3d_{x^2-y^2}$, $3d_{3z^2-r^2}$ orbitals by using Wannier downfolding of the density functional theory calculations, which captures the key ingredients of the material, such as band structure and Fermi surface topology. There are two electron pockets, α, β, and one hole pocket, γ, on the Fermi surface, in which the α, β pockets show mixing of two orbitals, while the γ pocket is associated with Ni-$d_{3z^2-r^2}$ orbital. The random phase approximation spin susceptibility reveals a magnetic enhancement associated with the $d_{3z^2-r^2}$ state. A higher energy model with O-p orbitals is also provided for further study.

DOI: 10.1103/PhysRevLett.131.126001

Introduction.—Recently, the newly discovered Ruddlesden-Popper bilayer perovskite nickelate $La_3Ni_2O_7$ shows a remarkable high superconducting transition temperature of $T_c \approx 80$ K with an applied pressure of over 14 GPa [1]. This breakthrough will undoubtedly cause a stir in the field of high-T_c superconductivity long after the discovery of suprate [2–7] and iron-based [8–11] superconductors, as well as the recent infinite layer nickelate superconductors [12–30]. At ambient pressure, $La_3Ni_2O_7$ exhibits an orthorhombic structure of the *Amam* space group [31]. With increasing pressure, it undergoes a structure transition to the *Fmmm* space group, which possesses a more regular AA-stacking structure with an apical Ni-O-Ni bond approaching 180° [see Figs. 1(f) and 1(g) in Ref. [1]]. The most crucial effect of the pressure is to drive a metallic transition of the correlated electronic ground state. The resistance measurement shows that, above T_c, $La_3Ni_2O_7$ undergoes a transition from weakly insulating to metallic phase [see Figs. 3(a) and 4 in Ref. [1]], which is further evidenced in the density functional theory (DFT) calculation as the emergence of an additional Ni-$d_{3z^2-r^2}$ state near Fermi energy (E_F) [1,32]. Such a state is essentially associated with the σ bonding that connects Ni-$d_{3z^2-r^2}$ and apical $O-p_z$ orbitals, further indicating a rather different situation in $La_3Ni_2O_7$ in which the unconventional pairing might be promoted by such a coupling degree [33–38]. Therefore, it is of vital importance to understand the effective low-energy physics.

In this Letter, we propose a bilayer two-orbital model and an eleven-orbital model for the high-pressure phase of $La_3Ni_2O_7$. Our models are constructed based on Wannier downfolding of the DFT band structure, which capture the key feature of the electronic structure at E_F and could serve as a starting point for further strongly correlated calculations and investigation on the unconventional pairing symmetry.

Electronic model.—To elucidate the electronic structure of $La_3Ni_2O_7$ under the high-pressure phase (29.5 Gpa), a primitive unit cell with two-Ni atoms is adopted. We fix the experimentally refined lattice parameters [1] and fully optimize the atomic positions using the DFT as implemented in the Vienna *ab initio* simulation package (VASP) [39,40]. The projector augmented-wave (PAW) method [41] with a 600 eV plane-wave cutoff is adopted. The generalized gradient approximation (GGA) of Perdew-Burke-Ernzerhof form (PBE) [42] is used for the exchange-correlation functional. In Fig. 1 we show the resulting band

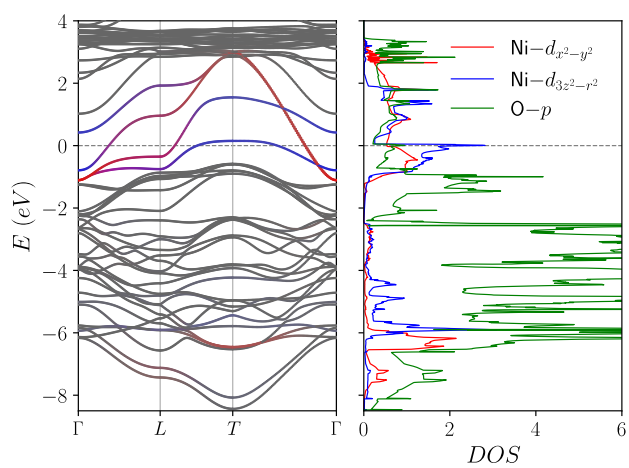

FIG. 1. The DFT band structure and partial density of states of the high-pressure *Fmmm* phase of $La_3Ni_2O_7$. The blue, red, and green colors represent Ni-$d_{x^2-y^2}$, $d_{3z^2-r^2}$, and O-p states, respectively.

structure and partial density of states, which distinctly shows major Ni-$d_{x^2-y^2}$ and $d_{3z^2-r^2}$ orbitals near E_F. Note that there appears a hole pocket associating the Ni-$d_{3z^2-r^2}$ orbital at the T point. This hole pocket is separated from the other one on the upper Fermi surface with an energy ~1.3 eV. This splitting should be attributed to $pd\sigma$ bonding between Ni-$d_{3z^2-r^2}$ and apical $O-p_z$ orbitals.

With the Wannier downfolding [43–45] of the DFT band structure, we arrive at an effective bilayer two-orbital model:

$$\begin{aligned}\mathcal{H} &= \mathcal{H}_0 + \mathcal{H}_U,\\ \mathcal{H}_0 &= \sum_{\mathrm{k}\sigma}\Psi^\dagger_{\mathrm{k}\sigma}H(\mathrm{k})\Psi_{\mathrm{k}\sigma},\\ \mathcal{H}_U &= U\sum_{is}n_{is\uparrow}n_{is\downarrow}\\ &\quad+\sum_{i\alpha\beta}(U'-J\delta_{\alpha\beta})(n_{iAx\alpha}n_{iAz\beta}+n_{iBx\alpha}n_{iBz\beta}).\end{aligned}\tag{1}$$

Here $\mathcal{H}_0$ is the tight-binding Hamiltonian determined out of our Wannier downfolding, and $\mathcal{H}_U$ is the Coulomb interaction term [46]. The basis is defined as $\Psi_\sigma = (d_{Ax\sigma}, d_{Az\sigma}, d_{Bx\sigma}, d_{Bz\sigma})^T$, with the field operator $d_{s\sigma}$ denotes annihilation of an $s = Ax, Az, Bx, Bz$ electron with spin σ. As shown in Fig. 2, A, B label the bilayer, and x, z label $d_{x^2-y^2}, d_{3z^2-r^2}$ orbitals, respectively. For $\mathcal{H}_U$, U, U', and J are Coulomb integrals of Kanamori parameterization with each representing intraorbital, interorbital Coulomb repulsion, and Hund's coupling, respectively. They are related by $U' = U - 2J$, reflecting Hund's rule. The matrix $H(\mathrm{k})$ is written as

$$\begin{aligned}H(\mathrm{k}) &= \begin{pmatrix} H_A(\mathrm{k}) & H_{AB}(\mathrm{k})\\ H_{AB}(\mathrm{k}) & H_B(\mathrm{k})\end{pmatrix},\\ H_A(\mathrm{k}) = H_B(\mathrm{k}) &= \begin{pmatrix} T^x_{\mathrm{k}} & V_{\mathrm{k}}\\ V_{\mathrm{k}} & T^z_{\mathrm{k}}\end{pmatrix},\quad H_{AB}(\mathrm{k}) = \begin{pmatrix} t^x_\perp & V'_{\mathrm{k}}\\ V'_{\mathrm{k}} & t^z_\perp\end{pmatrix},\end{aligned}\tag{2}$$

with

$$\begin{aligned}T^{x/z}_{\mathrm{k}} &= 2t^{x/z}_1(\cos k_x + \cos k_y) + 4t^{x/z}_2\cos k_x\cos k_y + \epsilon^{x/z},\\ V_{\mathrm{k}} &= 2t^{xz}_3(\cos k_x - \cos k_y),\quad V'_{\mathrm{k}} = 2t^{xz}_4(\cos k_x - \cos k_y).\end{aligned}$$

Here $T^{x/z}_{\mathrm{k}}$ represents intralayer intraorbital hopping, and V_{k} (V'_{k}) represent intralayer (interlayer) hybridization between $d_{x^2-y^2}$ and $d_{3z^2-r^2}$ orbitals. The essential hoppings $t^{x/z}_1, t^{x/z}_2, t^{xz}_3, t^{xz}_4$ are demonstrated in Fig. 2(a). Note that the minus sign appearing in the structure factor of t^{xz}_3, t^{xz}_4 is associated with the orbital symmetry of two e_g sectors.

To better illustrate the low-energy state, it is advisable to further simplify the above model. Recall that the mirror symmetry of the bilayer structure allows us to define the bonding and antibonding states $\Phi_{\pm\mathrm{k}\sigma} = (c^x_{\pm\mathrm{k}\sigma}, c^z_{\pm\mathrm{k}\sigma})^T$ with

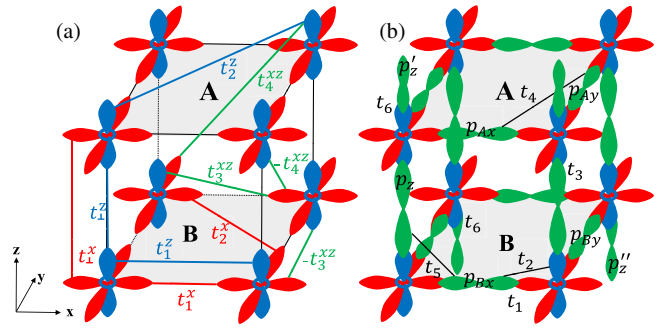

FIG. 2. Schematic of the bilayer $La_3Ni_2O_7$ lattice with hopping parameters. (a) Only Ni-$d_{x^2-y^2}$ (red), $d_{3z^2-r^2}$ (blue) orbitals are shown. The blue, red, and green lines indicate hoppings for the bilayer two-orbital model. Their values are listed in Table I. (b) Extra O-p orbitals are drawn as green shapes, with in-plane p_x, p_y and apical p_z, p'_z, p''_z. Some of the p'_z, p''_z are hidden for clarity. The hopping parameters are given in Table II.

$c^{x/z}_{\pm\mathrm{k}\sigma} = (1/\sqrt{2})(d^{x/z}_{\mathrm{k}A\sigma} \pm d^{x/z}_{\mathrm{k}B\sigma})$, in which the Hamiltonian acquires a block-diagonal form

$$\begin{aligned}\mathcal{H}_0 &= \sum_{\mathrm{k}\sigma}\left(\Phi^\dagger_{+\mathrm{k}\sigma}H_+(\mathrm{k})\Phi_{+\mathrm{k}\sigma} + \Phi^\dagger_{-\mathrm{k}\sigma}H_-(\mathrm{k})\Phi_{-\mathrm{k}\sigma}\right),\\ H_\pm(\mathrm{k}) &= \begin{pmatrix} T^x_{\mathrm{k}} \pm t^x_\perp & V_{\mathrm{k}} \pm V'_{\mathrm{k}}\\ V_{\mathrm{k}} \pm V'_{\mathrm{k}} & T^z_{\mathrm{k}} \pm t^z_\perp\end{pmatrix}.\end{aligned}\tag{3}$$

In this representation, the bonding and antibonding states of two $d_{3z^2-r^2}$ orbitals at E_F are manifested as the component $T^z_{\mathrm{k}} \pm t^z_\perp$ which define a splitting energy $2|t^z_\perp|$, as shown along the M-Γ path in Fig. 3 (where $V_{\mathrm{k}}, V'_{\mathrm{k}} = 0$).

With the value of tight-binding parameters listed in Table I, we show in Fig. 3 the resulting band structure and Fermi surface. The model reproduces the DFT band structure well at E_F. Also, site energies are slightly adjusted to coincide with the nominal $d^{7.5}$ configuration [1,32]. In Fig. 3(b) we can see two electron pockets, α, β, and one hole pocket, γ. The α, β pockets show mixing of the orbital content, while the γ pocket is featured as a dominated $d_{3z^2-r^2}$ state. Note that the amplitude of $t^z_\perp = -0.635$ is even larger than that of the intralayer nearest-neighbor

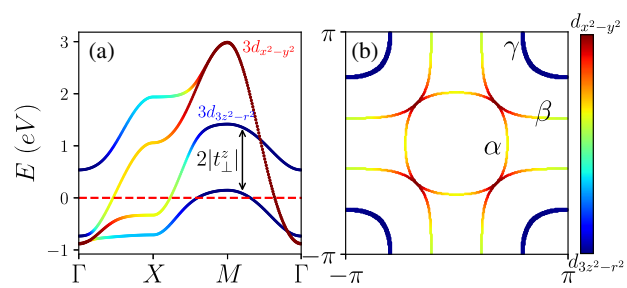

FIG. 3. The band structure (a) and Fermi surface (b) of the bilayer two-orbital model. The color bar indicates the orbital weight of $d_{x^2-y^2}$ and $d_{3z^2-r^2}$.

TABLE I. Tight-binding parameters of the bilayer two-orbital model. The hoppings t are demonstrated in Fig. 2(a). ϵ^x, ϵ^z are site energies for Ni-$d_{x^2-y^2}$, $d_{3z^2-r^2}$ orbitals, respectively. The units are eV.

t_1^x	t_1^z	t_2^x	t_2^z	t_3^{xz}
−0.483	−0.110	0.069	−0.017	0.239
$t_\perp^x$	$t_\perp^z$	t_4^{xz}	ϵ^x	ϵ^z
0.005	−0.635	−0.034	0.776	0.409

hopping $t_1^x = -0.483$, by a ratio of 1.3. This strong interlayer coupling indicates a possible different situation of the unconventional paring as compared to cuprates, and is reminiscent of a theoretical bilayer-Hubbard model [47,48], in which an $s_\pm$-wave pairing could be promoted via interlayer coupling. But there is a key difference here. In $La_3Ni_2O_7$, $t_\perp^z$ only appears in the $d_{3z^2-r^2}$ sector, while for $d_{x^2-y^2}$ the amplitude $t_\perp^x = 0.005$ is marginal. Hence, the influence from interlayer coupling to the NiO_2 plane can only be achieved via hybridizations V_k, V'_k. It would be interesting to see how pairing symmetry is affected in this situation. We would also like to point out that, however, due to the asymmetry of the orthorhombic structure of this compound, the γ pocket from DFT is slightly stretched along the nodal direction.

To explicitly consider the physics of O-p orbitals, we introduce a higher energy model (eleven-orbital model). The basis is $\Psi = (d_{Ax}, d_{Az}, d_{Bx}, d_{Bz}, p_{Ax}, p_{Ay}, p_{Bx}, p_{By}, p_z, p'_z, p''_z)^T$, with four more in-plane, $p_{Ax}, p_{Ay}, p_{Bx}, p_{By}$, and three apical p_z, p'_z, p''_z, as shown in Fig. 2(b). The tight-binding parameters of the model are listed in Table II, which requires six hopping parameters including necessary pd, pp overlaps. The resulting band structure covers an energy range akin to that of Fig. 1 and can also reproduce the main features at E_F. Moreover, we found a strong hopping of $t_6 = 1.366$ between $d_{3z^2-r^2}$ and two apical p'_z, p''_z that lie outside the bilayer, which manifest as two hole baths for the NiO_2 plane and could be further integrated out in a Löwdin downfolding technique [49]. The model will be useful for further study of the electronic correlation in the dynamic mean field theory framework.

TABLE II. Tight-binding parameters for Wannier downfolding of the eleven-orbital model. $\epsilon^{x/z}$ are site energies for $d_{x^2-y^2}/d_{3z^2-r^2}$, and $\epsilon_p^{x/y}$ for in-plane p_x/p_y, and $\epsilon^z_{p/p'/p''}$ for apical $p_z/p'_z/p''_z$. See Fig. 2(b) for details. The units are eV.

t_1	t_2	t_3	t_4	t_5	t_6
−1.564	0.747	−1.625	0.577	−0.487	1.366
ϵ^x	ϵ^z	$\epsilon_p^{x/y}$	ϵ_p^z	$\epsilon^z_{p'/p''}$	
−1.057	−1.161	−4.936	−4.294	−3.772	

Spin susceptibility.—To determine the magnetic response of the material, we investigate the spin susceptibility of our model, which is defined as

$$\chi_S^{st}(q, i\omega_n) = \frac{1}{3}\int_0^\beta d\tau e^{i\omega_n\tau}\langle \boldsymbol{S}_s(q,\tau)\cdot\boldsymbol{S}_t(-q,0)\rangle. \quad (4)$$

Here $s, t = Ax, Az, Bx, Bz$ label orbitals, and the spin operator is defined as $\boldsymbol{S}_{qs} = \frac{1}{2}\sum_{\mathrm{k}\alpha\beta} d^\dagger_{\mathrm{k}s\alpha}\boldsymbol{\sigma}_{\alpha\beta}d_{\mathrm{k}+qs\beta}$ with $\boldsymbol{\sigma}$ the Pauli matrix. By using wick's theorem, we expand Eq. (4) to obtain the bare (noninteracting) susceptibility

$$\chi_S^{st}(q, i\omega_n) = -\frac{1}{2N}\sum_{mn}\frac{f(\epsilon^n_\mathrm{k}) - f(\epsilon^m_\mathrm{k})}{i\omega_n + \epsilon^n_\mathrm{k} - \epsilon^m_{\mathrm{k}+\mathrm{q}}} \times \langle m|\mathrm{k}+qt\rangle\langle \mathrm{k}+qs|m\rangle\langle n|\mathrm{k}s\rangle\langle \mathrm{k}t|n\rangle,$$

with m, n the band indices and $f(\epsilon) = 1/(e^{\epsilon/T}+1)$ the Fermi-Dirac function. $\langle \mathrm{k}s|m\rangle$ represents the eigenvector relating s, m states at wave vector k.

Under the random phase approximation, the spin susceptibility is calculated by

$$\chi_S^{st,\mathrm{RPA}}(q, i\omega_n) = [I - \chi_S^{st}(q, i\omega_n)\Gamma]^{-1}\chi_S^{st}(q, i\omega_n), \quad (5)$$

with the interaction vertex defined as

$$\Gamma = \begin{pmatrix} 1 & \\ & 1 \end{pmatrix} \otimes \begin{pmatrix} U & J/2 \\ J/2 & U \end{pmatrix}.$$

In Fig. 4 we show the constant energy slices of $\chi_S^\mathrm{RPA}(q, \omega = 0)$. Here we use $U = 3$, $J = 0.4$ eV. $T = 0$ is applied since the temperature only trivially brings a broadening to the spectrum. Figure 4(a) is the total $\chi_S^\mathrm{RPA} = \sum_{s,t}\chi_S^{st,\mathrm{RPA}}$ corresponding to the experimental measurable. As can be seen, the magnetic signal shows a ringlike enhancement. To unveil the origin, we show in Figs. 4(b)–4(d) the orbital-resolved $\chi_S^{st,\mathrm{RPA}}$, from which we can see a dominated intraorbital $d_{3z^2-r^2}$ scattering reflecting Fermi surface nesting of the γ pocket. While the signals from the other two channels are weaker, consistent with the strong orbital mixing in α, β pockets. Our result could be further tested in the magnetic measurement.

Discussion.—The discovery of the high transition temperature superconductor $La_3Ni_2O_7$ represents a major breakthrough in the field of nickletate superconductivity. Our DFT calculations demonstrate that there are two electron pockets, α, β, and one hole pocket, γ, on the Fermi surface, in which the α, β pockets exhibit mixing of orbitals, while the γ pocket features a dominated $d_{3z^2-r^2}$ content. In comparison to the bulk Ni-112, which has not yet demonstrated a finite T_c, $La_3Ni_2O_7$ exhibits several distinguishing features that may be crucial to superconductivity. First, the less correlated

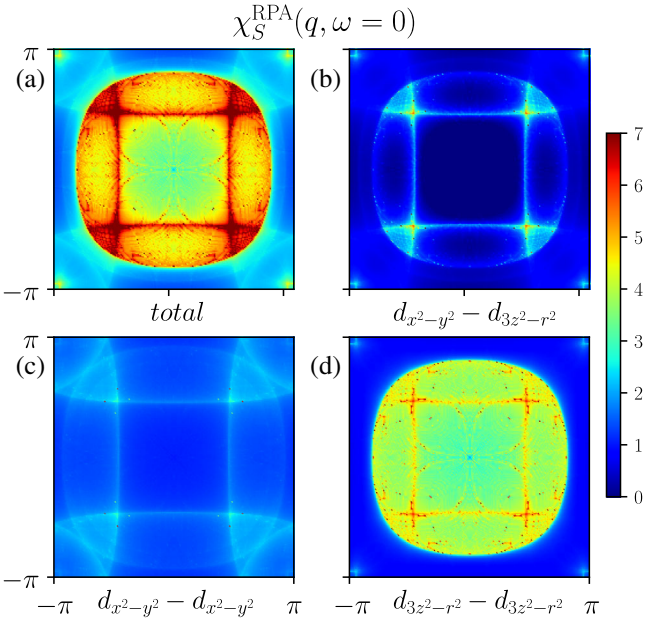

FIG. 4. Spin susceptibility $\chi_S^{st,\mathrm{RPA}}(q,\omega=0)$ of the bilayer two-orbital model. (a) The total orbital sum $\chi_S^{\mathrm{RPA}}=\sum_{st}\chi_S^{st,\mathrm{RPA}}$ which corresponds to the experimental measurable. [(b)–(d)] Orbital-resolved $\chi^{st,\mathrm{RPA}}$. An amplified factor of 2 is used in (b) and (c).

La-5d derived bands are expelled from the Fermi level, diminishing the hybridization between the Ni-3$d_{x^2-y^2}$ and La-5d orbitals that impedes superconductivity. Furthermore, the site energy difference between Ni-$d_{x^2-y^2}(\epsilon^x)$ and O-$p(\epsilon_p^{x/y})$ in $La_3Ni_2O_7$ is estimated as $\Delta\equiv\epsilon^x-\epsilon_p^{x/y}=3.88$ eV (see Table II). This value is smaller than that of $RNiO_2$ (4.4 eV) [16], which could potentially contribute to the high T_c in $La_3Ni_2O_7$ in the context of pairing based on the Zhang-Rice singlet state [50]. The inclusion of the $d_{3z^2-r^2}$ orbital near Fermi level in $La_3Ni_2O_7$, however, may have complex implications for superconductivity. The large density of state of the $d_{3z^2-r^2}$ orbital can provide new phase space for the potential pairing of electrons [51]. However, the presence of multiple orbitals on the Fermi level may also lead to competition between pairings with different symmetries, such as the competition between the $s_\pm$ and $d_{x^2-y^2}$ wave pairing. Regarding the filling factors of the relevant orbitals, we note that in the case of a $d^{7.5}$ configuration of Ni, if $d_{3z^2-r^2}$ is considered to roughly have the same occupation number as of $d_{x^2-y^2}$, then both orbitals have about 0.75 electrons per site, corresponding to 25% hole doping. It is notable that the oxygen deficiency in realistic materials may effectively reduce the hole doping level in the e_g orbitals of Ni 3d, resulting in enhanced superconductivity. Finally, we acknowledge that the $d_{3z^2-r^2}$ orbitals exhibit much weaker hybridization with in-plane oxygen compared to its $d_{x^2-y^2}$ counterpart, which necessitates in-depth investigations into its strong interaction effects and its influence on superconductivity. The question about the role of the electron-phonon coupling, which becomes specifically important since the superconductivity in $La_3Ni_2O_7$ is found under pressure, should also be clarified in future studies.

Conclusion.—In conclusion, we have introduced a minimal bilayer two-orbital model and an eleven-orbital model for the Ruddlesden-Popper bilayer $La_3Ni_2O_7$ under pressure. The tight-binding parameters are obtained by Wannier downfolding of the DFT calculations, which reproduce the band structure and Fermi surface well. The spin susceptibility is studied using the RPA method, which shows that the magnetic signal majorly comes from $d_{3z^2-r^2}$. These models provide important means to study the electronic, magnetic, orbital, and superconducting properties of the material under pressure.

We are thankful for the useful discussions with Guang-Ming Zhang, Biao Lv, and Yusheng Hou. Work at Sun Yat-Sen University was supported by the National Key Research and Development Program of China (Grants No. 2022YFA1402802, 2018YFA0306001), the National Natural Science Foundation of China (Grants No. 92165204, No. 12174454, No. 11974432, No. 12274472), the Guangdong Basic and Applied Basic Research Foundation (Grants No. 2022A1515011618, No. 2021B1515120015), Guangdong Provincial Key Laboratory of Magnetoelectric Physics and Devices (Grant No. 2022B1212010008), Shenzhen International Quantum Academy (Grant No. SIQA202102), and Leading Talent Program of Guangdong Special Projects (201626003).

Z. L. and X. H. contributed equally to this work.

Note added.—Recently, we noticed several later works [52–55] showing consistency with our results and Ref. [56] adopted our model to reveal a possible $s_\pm$-wave pairing in the material.

*yaodaox@mail.sysu.edu.cn

[1] H. Sun, M. Huo, X. Hu, J. Li, Y. Han, L. Tang, Z. Mao, P. Yang, B. Wang, J. Cheng *et al.*, SSignatures of superconductivity near 80 K in a nickelate under high pressure, Nature (2023).

[2] J. G. Bednorz and K. A. Müller, Possible high T_c superconductivity in the Ba-La-Cu-O system, Z. Phys. B Condens. Matter **64**, 189 (1986).

[3] P. W. Anderson, The resonating valence bond state in La_2CuO_4 and superconductivity, Science **235**, 1196 (1987).

[4] P. A. Lee, N. Nagaosa, and X.-G. Wen, Doping a mott insulator: Physics of high-temperature superconductivity, Rev. Mod. Phys. **78**, 17 (2006).

[5] B. Keimer, S. A. Kivelson, M. R. Norman, S. Uchida, and J. Zaanen, From quantum matter to high-temperature superconductivity in copper oxides, Nature (London) **518**, 179 (2015).

[6] H. Sakakibara, K. Suzuki, H. Usui, S. Miyao, I. Maruyama, K. Kusakabe, R. Arita, H. Aoki, and K. Kuroki, Orbital mixture effect on the fermi-surface–T_c correlation in the cuprate superconductors: Bilayer vs. single layer, Phys. Rev. B **89**, 224505 (2014).

[7] W. Li, J. Zhao, L. Cao, Z. Hu, Q. Huang, X. Wang, Y. Liu, G. Zhao, J. Zhang, Q. Liu *et al.*, Superconductivity in a unique type of copper oxide, Proc. Natl. Acad. Sci. U.S.A. **116**, 12156 (2019).

[8] S. Raghu, X.-L. Qi, C.-X. Liu, D. J. Scalapino, and S.-C. Zhang, Minimal two-band model of the superconducting iron oxypnictides, Phys. Rev. B **77**, 220503(R) (2008).

[9] A. V. Chubukov, D. V. Efremov, and I. Eremin, Magnetism, superconductivity, and pairing symmetry in iron-based superconductors, Phys. Rev. B **78**, 134512 (2008).

[10] H. Eschrig and K. Koepernik, Tight-binding models for the iron-based superconductors, Phys. Rev. B **80**, 104503 (2009).

[11] M. Daghofer, A. Nicholson, A. Moreo, and E. Dagotto, Three orbital model for the iron-based superconductors, Phys. Rev. B **81**, 014511 (2010).

[12] D. Li, K. Lee, B. Y. Wang, M. Osada, S. Crossley, H. R. Lee, Y. Cui, Y. Hikita, and H. Y. Hwang, Superconductivity in an infinite-layer nickelate, Nature (London) **572**, 624 (2019).

[13] E. Been, W.-S. Lee, H. Y. Hwang, Y. Cui, J. Zaanen, T. Devereaux, B. Moritz, and C. Jia, Electronic Structure Trends Across the Rare-Earth Series in Superconducting Infinite-Layer Nickelates, Phys. Rev. X **11**, 011050 (2021).

[14] K.-W. Lee and W. E. Pickett, Infinite-layer $LaNiO_2$: Ni^{1+} is not Cu^{2+}, Phys. Rev. B **70**, 165109 (2004).

[15] M. Hepting, D. Li, C. Jia, H. Lu, E. Paris, Y. Tseng, X. Feng, M. Osada, E. Been, Y. Hikita *et al.*, Electronic structure of the parent compound of superconducting infinite-layer nickelates, Nat. Mater. **19**, 381 (2020).

[16] A. S. Botana and M. R. Norman, Similarities and Differences between $LaNiO_2$ and $CaCuO_2$ and Implications for Superconductivity, Phys. Rev. X **10**, 011024 (2020).

[17] X. Wu, D. Di Sante, T. Schwemmer, W. Hanke, H. Y. Hwang, S. Raghu, and R. Thomale, Robust $d_{x^2-y^2}$-wave superconductivity of infinite-layer nickelates, Phys. Rev. B **101**, 060504(R) (2020).

[18] M. Jiang, M. Berciu, and G. A. Sawatzky, Critical Nature of the Ni Spin State in Doped $NdNiO_2$, Phys. Rev. Lett. **124**, 207004 (2020).

[19] L.-H. Hu and C. Wu, Two-band model for magnetism and superconductivity in nickelates, Phys. Rev. Res. **1**, 032046 (R) (2019).

[20] Y. Nomura, M. Hirayama, T. Tadano, Y. Yoshimoto, K. Nakamura, and R. Arita, Formation of a two-dimensional single-component correlated electron system and band engineering in the nickelate superconductor $NdNiO_2$, Phys. Rev. B **100**, 205138 (2019).

[21] Y.-H. Zhang and A. Vishwanath, Type-II $t-J$ model in superconducting nickelate $Nd_{1-x}Sr_xNiO_2$, Phys. Rev. Res. **2**, 023112 (2020).

[22] P. Werner and S. Hoshino, Nickelate superconductors: Multiorbital nature and spin freezing, Phys. Rev. B **101**, 041104(R) (2020).

[23] F. Bernardini, V. Olevano, and A. Cano, Magnetic penetration depth and T_c in superconducting nickelates, Phys. Rev. Res. **2**, 013219 (2020).

[24] Y. Gu, S. Zhu, X. Wang, J. Hu, and H. Chen, A substantial hybridization between correlated Ni-d orbital and itinerant electrons in infinite-layer nickelates, Commun. Phys. **3**, 84 (2020).

[25] M. Kitatani, L. Si, O. Janson, R. Arita, Z. Zhong, and K. Held, Nickelate superconductors–a renaissance of the one-band Hubbard model, npj Quantum Mater. **5**, 59 (2020).

[26] F. Lechermann, Doping-dependent character and possible magnetic ordering of $NdNiO_2$, Phys. Rev. Mater. **5**, 044803 (2021).

[27] A. Kreisel, B. M. Andersen, A. T. Rømer, I. M. Eremin, and F. Lechermann, Superconducting Instabilities in Strongly Correlated Infinite-Layer Nickelates, Phys. Rev. Lett. **129**, 077002 (2022).

[28] F. Lechermann, Multiorbital Processes Rule the $Nd_{1-x}Sr_xNiO_2$ Normal State, Phys. Rev. X **10**, 041002 (2020).

[29] N. Kitamine, M. Ochi, and K. Kuroki, Designing nickelate superconductors with d^8 configuration exploiting mixed-anion strategy, Phys. Rev. Res. **2**, 042032(R) (2020).

[30] G.-M. Zhang, Y.-f. Yang, and F.-C. Zhang, Self-doped mott insulator for parent compounds of nickelate superconductors, Phys. Rev. B **101**, 020501(R) (2020).

[31] Z. Liu, H. Sun, M. Huo, X. Ma, Y. Ji, E. Yi, L. Li, H. Liu, J. Yu, Z. Zhang *et al.*, Evidence for charge and spin density waves in single crystals of $La_3Ni_2O_7$ and $La_3Ni_2O_6$, Sci. China Phys. Mech. Astron. **66**, 217411 (2023).

[32] V. Pardo and W. E. Pickett, Metal-insulator transition in layered nickelates $La_3Ni_2O_{7-\delta}$ ($\delta = 0.0, 0.5, 1$), Phys. Rev. B **83**, 245128 (2011).

[33] H. J. Choi, D. Roundy, H. Sun, M. L. Cohen, and S. G. Louie, The origin of the anomalous superconducting properties of MgB_2, Nature (London) **418**, 758 (2002).

[34] M. Gao, Z.-Y. Lu, and T. Xiang, Prediction of phonon-mediated high-temperature superconductivity in $Li_3B_4C_2$, Phys. Rev. B **91**, 045132 (2015).

[35] A. Drozdov, P. Kong, V. Minkov, S. Besedin, M. Kuzovnikov, S. Mozaffari, L. Balicas, F. Balakirev, D. Graf, V. Prakapenka *et al.*, Superconductivity at 250 K in lanthanum hydride under high pressures, Nature (London) **569**, 528 (2019).

[36] M. Gao, Z. Lu, and T. Xiang, Finding high-temperature superconductors by metallizing the σ-bonding electrons, Physics **44**, 421 (2015).

[37] J. Hu, Identifying the genes of unconventional high temperature superconductors, Sci. Bull. **61**, 561 (2016).

[38] J. Hu, C. Le, and X. Wu, Predicting Unconventional High-Temperature Superconductors in Trigonal Bipyramidal Coordinations, Phys. Rev. X **5**, 041012 (2015).

[39] G. Kresse and J. Hafner, *Ab initio* molecular dynamics for liquid metals, Phys. Rev. B **47**, 558 (1993).

[40] G. Kresse and J. Furthmüller, Efficient iterative schemes for *ab initio* total-energy calculations using a plane-wave basis set, Phys. Rev. B **54**, 11169 (1996).

[41] P. E. Blöchl, Projector augmented-wave method, Phys. Rev. B **50**, 17953 (1994).

[42] J. P. Perdew, K. Burke, and M. Ernzerhof, Generalized Gradient Approximation Made Simple, Phys. Rev. Lett. **77**, 3865 (1996).

[43] G. Pizzi *et al.*, Wannier90 as a community code: New features and applications, J. Phys. Condens. Matter **32**, 165902 (2020).

[44] N. Marzari and D. Vanderbilt, Maximally localized generalized Wannier functions for composite energy bands, Phys. Rev. B **56**, 12847 (1997).

[45] I. Souza, N. Marzari, and D. Vanderbilt, Maximally localized Wannier functions for entangled energy bands, Phys. Rev. B **65**, 035109 (2001).

[46] A. Georges, L. d. Medici, and J. Mravlje, Strong correlations from hunds coupling, Annu. Rev. Condens. Matter Phys. **4**, 137 (2013).

[47] T. A. Maier and D. J. Scalapino, Pair structure and the pairing interaction in a bilayer Hubbard model for unconventional superconductivity, Phys. Rev. B **84**, 180513(R) (2011).

[48] M. Nakata, D. Ogura, H. Usui, and K. Kuroki, Finite-energy spin fluctuations as a pairing glue in systems with coexisting electron and hole bands, Phys. Rev. B **95**, 214509 (2017).

[49] P. Löwdin, A note on the quantum mechanical perturbation theory, J. Chem. Phys. **19**, 1396 (2004).

[50] F. C. Zhang and T. M. Rice, Effective Hamiltonian for the superconducting Cu oxides, Phys. Rev. B **37**, 3759 (1988).

[51] J. Hu and H. Ding, Local antiferromagnetic exchange and collaborative fermi surface as key ingredients of high temperature superconductors, Sci. Rep. **2**, 381 (2012).

[52] Y. Zhang, L.-F. Lin, A. Moreo, and E. Dagotto, Electronic structure, orbital-selective behavior, and magnetic tendencies in the bilayer nickelate superconductor $La_3Ni_2O_7$ under pressure, arXiv:2306.03231.

[53] Y. Gu, C. Le, Z. Yang, X. Wu, and J. Hu, Effective model and pairing tendency in bilayer Ni-based superconductor $La_3Ni_2O_7$, arXiv:2306.07275.

[54] Y. Shen, M. Qin, and G.-M. Zhang, Effective bi-layer model Hamiltonian and density-matrix renormalization group study for the high-Tc superconductivity in $La_3Ni_2O_7$ under high pressure, arXiv:2306.07837.

[55] H. Sakakibara, N. Kitamine, M. Ochi, and K. Kuroki, Possible high T_c superconductivity in $La_3Ni_2O_7$ under high pressure through manifestation of a nearly-half-filled bilayer Hubbard model, arXiv:2306.06039.

[56] Q.-G. Yang, D. Wang, and Q.-H. Wang, Possible $S_{\pm}$-wave superconductivity in $La_3Ni_2O_7$, arXiv:2306.03706.